AMSE Association for the Advancement of Modelling & Simulation Techniques in Enterprises
IIETA International Information and Engineering Technology Association
Advancing the World of Information and Engineering

Advances in Modelling and Analysis A
Vol. 55, No. 3, September, 2018, pp. 177-185
Journal homepage: http://iieta.org/Journals/AMA/AMA_A

Design of heliostat field for an unfired solarized micro gas turbine in a closed cycle with mass flow control regulation

F. Rovense[1*], M. Bomentre[1], M.S. Silva[2], V. Ferraro[2], M. Amelio[1]

[1] Department of Mechanical, Energy and Management Engineering, University of Calabria, Via P. Bucci Edificio Cubo 46 C, 87063, Arcavacata di Rende (CS) Rende, Italy
[2] Department of Energy Engineer, Escuela Técnica Superior de Ingeniería Universidad de Sevilla, Camino de los Descubrimientos, s/n. 41092 Sevilla, Spain

Corresponding Author Email: francesco.rovense@unical.it

https://doi.org/10.18280/ama_a.550312

Received: 18 March 2018
Accepted: 28 May 2018

Keywords:
concentrating solar power, micro gas turbine, csps, control system, heliostats

ABSTRACT

Interest in smart networks has increased over the past decade. One of the main advantages is the possibility of producing electricity on site and autonomously. In this scenario, small or very small generators, installed near of the places of consumption, play a fundamental role. A real possibility is offered by the Gas Micro-turbine (MGT). Such a machine has the possibility to follow the electric load of the network and is also suitable to use solar energy as a source of heat in the cycle, through the concentration of direct normal radiation (DNI). With the solar power supply, the regulation capacity of the MGT can be exploited in order to convert all the thermal power collected.
In this work, the solar field, of an unfired closed solarized micro gas turbine employing air as working fluid with mass flow control system, has been analyzed. The mass flow control system is able to adjust the mass flow rate by means of a variation in density, to control the turbine inlet temperature (TIT), as the incoming thermal power varies. The volumes of the engine, as well as the speed triangles, do not change; therefore, by keeping a TIT constant, it is possible to control the power production, according to the incident solar radiation, without a degradation of efficiency. The concentrating solar tower and receiver systems are able to produce thermal power suitable in MGT and in this case represent the only one heat source. The heliostats field control system operates together with the mass flow one, so the optimization of the solar field plays a fundamental role in controlling the TIT and increasing the energy production. The aim of this work is the design of the heliostats field able to control the TIT with the mass flow control system and which is suitable, as heat source, to increase the energy production. Different heliostats size and solar multiple (SM) have been taken in to account to choose the best configuration of the solar field. The analysis has been carried out by the open source Solar PILOT, while the weather data of Seville town have been considered. The results show that the heliostats field best configuration allows getting a substantial energy production and let to adjust the solar flux precisely in order to control, with the mass flow control system, the TIT.

1. INTRODUCTION

Nowadays, the primary energy demand has increased, rising up to 62.5% compared to 20 years ago. The necessity of the renewable sources has prompted the government policies, around the world, to encourage the development of new energy production systems at first to reduce National Power Grid impact [1]. The solar energy appears the most suitable source for this scope. It is clear that the measurement [2] and prediction [3] of the energy available plays a fundamental role.

Moreover, its integration in different sectors such as buildings by means of hybrid energy systems [4] or handling its excess by means of storage technologies [5] are getting attention within the scientific community.

The Concentrating Solar Power system (CSPs), is a technology that concentrates the solar radiation making it available, through a heat transfer fluid (HTF), as a heat source in a power thermodynamic cycle. The most efficient power cycle, as we know is the Joule-Brayton one, that in a closed configuration allows to use different HTF; in addition, it is possible to work under pressurized conditions [6]. The use of the air, as HTF, in MGT with CSTs was explored [7], and in addition the employ of Thermal Energy Storage was also analyzed [8].

This option is among the most attractive alternatives for the replacement of natural gas in electrical industrial applications and goes in the same direction as what is proposed in the civil field [9] for the containment of CO_2 emissions.

The parametric analysis of the solar field for the unfired closed Joule Brayton cycle was conducted for different size power rate of the gas turbine [10] and the optimization of the best SM was carried out [11].

In this work the design of the heliostats field for a solarized micro gas turbine of a peak power of 500 kW with mass flow regulation system will be carried out. Particular attention will be paid to the solar multiple (SM) and the heliostats sizes.

Several manufacturers of micro gas turbine were taken into account with the MTG products [12].

For the purposes of the calculation, the technical data of the Ansaldo Turbec T 100 were then considered [13]. The same turbine, conveniently customized, is employed in Aora Solar system [14].

Increasing the pressure base of the gas turbine, it is possible to rise up its peak power. In this case, a pressurization of 5 time was supposed, due to the mechanical resistance of the solar receiver.

2. METHODOLOGY

As above mentioned, the heliostat field design was carried out by SolarPilot (Solar Power Tower Integrated Layout and Optimization Tool). SolarPILOT TM is a software able to generate and defines the characteristics of the central receiver systems and which was developed by National Renewable Energy Laboratory (NREL) [15].

The focus analysis is the choice of the best configuration in term of the heliostat size and solar multiple, suitable for the pressurized micro gas turbine.

2.1 Heliostats field parametric analysis

In this part, the optimization for different solar multiple (from 1 to 1.3) and heliostat size will be performed, in order to maximize the overall cycle efficiency. First, it is necessary to choose the model to approximate the emission of radiation by the Sun, [16]; in this case was select the Limb-Darkened Sun, where the solar radiation φ is the function of the angular distance θ between the point considered and the centroid of the solar disk according to the following equation:

$$\phi(\theta) = 1 - 0{,}5138\ \left(\frac{\theta}{0{,}00465}\right)^4 \quad (1)$$

For the atmospheric attenuation it has been employed Delsol3 Clear Day, which provides a visibility of 23 km in for a clear day, for the DNI density, and TMY data of Seville [17] for the meteorological data.

It was necessary to evaluate the engine cycle efficiency, imposed equal to 30%, and the auxiliary yield equal to 97%.

The code calculates the gross and net power of the cycle as:

$$\dot{W}_{cycle} = \dot{Q}_{pb} \cdot \eta_{cycle} \quad (2)$$

$$\dot{W}_{net} = \dot{W}_{cycle} \cdot \eta_{aux} \quad (3)$$

where:

$\dot{W}_{cycle}$ is the gross power of the cycle;

(1) $\dot{Q}_{pb}$ is the power needed for the power block;

(2) η_{cycle} is the referring efficiency of the power block;

(3) $\dot{W}_{net}$ is the net power;

(4) η_{aux} is the auxiliary efficiency.

The code evaluates also the net power of the heliostats field:

$$\dot{Q}_{field} = \dot{Q}_{inc}\,\alpha - \dot{Q}_{loss} - \dot{Q}_{pipe} \quad (4)$$

where:

(1) $\dot{Q}_{inc}$ is the power incident on the heliostats;

(2) α is the absorbance of the receiver;

(3) $\dot{Q}_{loss}$ are the radiative losses;

(4) $\dot{Q}_{pipe}$ are the pipe losses.

In table 1, the net power absorbed by the solar is resumed field for different solar multiple.

Table 1. Power absorbed by solar fields

SM	Q_{field}
1	1.7
1.1	1.87
1.2	2.04
1.3	2.2

It is also necessary to define two angles; the first one is the angle at the top of heliostats position, calculated in an anticlockwise direction, while the second represents the angle below of heliostats position, calculated in a clockwise direction. Both were imposed to 180 °.

By setting the radial limits of the field, it is possible to choose boundaries condition on the height of the tower (Ht); in this case it was chosen a minimum distance of 0.75 Ht and as a maximum 7.5 Ht.

The field configuration considered is the radial stagger layout, while as radial spacing method the "No Blocking-dense" has been selected, because it minimizes the blocking effect between the rows.

It has also been imposed the azimuthal spacing limit, equal to 1.33 [18].

It is necessary to define the geometry of the heliostats, defining the height Hh and width Wh, if the heliostat is composed by multiple panels, the number of panels in the horizontal and vertical directions and the space between the panels in every direction.

The software, via the height and width of the heliostats, calculates the diagonal dimension Dh as:

$$D_h = \sqrt{{W_h}^2 + {H_h}^2} \quad (5)$$

Another important parameter to design the heliostat field is the canting method. The methodology for this process is not unique, but it is possible to classify into two main groups: "on-axis" "off-axis" [19]. In the first case, the panels are aligned to give a perfect reflection of the image when the center of the heliostat, the receiver, and the Sun are all aligned; in the second case, the panels are arranged to optimize the convergence of all the reflected images on the solar receiver for a particular time of the year.

The methodology chosen for optimization is "On-Axis at Slant": where the panels are aligned when the heliostat reflects on the tower. The parameters chosen for the focusing of the heliostats are the kind “At Slant” in which the focusing distance of the heliostat is equal to the distance between the centroid of the heliostat and that of the receiver.

All the heliostats are characterized by optical errors, due to the uncertainty of the tracking system, along the σel and azimuthal σaz zenithally directions. Other are caused by the distortion of the surface along directions x σ (s, x) and σ(s, y) and the reflection of solar radiation, along the directions x σ(r, x) and σ(r, y), which are influenced by the wind, the gravity and the temperature. SolarPILOT assumes a normal distribution of these magnitudes and the user can set them by inserting the standard deviation of each individual magnitude. The software then goes to calculate the actual standard deviation of the image reflected by the heliostat σtot considering all error sources:

$$\sigma_{tot} = \sqrt{4\left({\sigma_{el}}^2 + {\sigma_{az}}^2 + {\sigma_{s,x}}^2 + {\sigma_{s,y}}^2\right) + {\sigma_{r,x}}^2 + {\sigma_{r,y}}^2} \quad (6)$$

The σel and σaz values have been chosen equal to 0 while for σ(r, x) and σ(r, y) a value that could range between 1.3 to 2.6 mrad have been selected. The surface distortion, instead, varies for each type of heliostat.

Then the reflectivity ratio, i.e. the ratio between the effective reflective area of the mirror and the total area, the reflectivity of the heliostat and the fouling factor, relative to the reflection of the heliostat when it is not perfectly clean has been chosen, and is was selected from 95% to 92% [18].

As already mentioned, three different types of heliostat (Type 1. large size, Type 2 intermediate sizes, Type 3 small size) have been analyzed and then a comparison has been made in order to evaluate which of them worked best for the plant. The heliostats data are shown in Table 2 [19].

Table 2. Characteristic data of heliostats

	Type 1	Type 2	Type 3
Area [m^2]	115.56	43.33	16.69
Height [m]	9	6.42	3.21
Length [m]	12.84	6.75	5.2
Number of panel X direction [-]	4	3	2
Number of panel Y direction [-]	4	2	1
Surface reflectivity ratio [-]	0.9583	0.97	0.92
Optical error [mrad]	2.6	1.8	1.3

2.2 Solar receiver

n this part the receiver design will be analyzed for the micro gas turbine application. First of all, a flat plate receiver has been selected in SolarPilot, so height and length of this component have been chosen to evaluate the receiver area.

Then it has been imposed the average incident flux on the receiver, elected equal to 400 kW/m2 [20], the maximum one of 600 kW/m2 and an absorbance of 0.96, (because it was supposed that it was a silicon carbide absorber) [21]. After this evaluation, the power to heat the working fluid was the following:

$$P_{wf} = \frac{P_{net}}{\eta_{cycle}\eta_{aux}} \quad (7)$$

The incident power on the receiver has been calculated as:

$$P_{Inc,rec} = \frac{SM \cdot P_{wf}}{\eta_{th,ric}} \quad (8)$$

The ratio between the incident power on the receiver and the average flux is the absorber area:

$$A = \frac{P_{Inc,rec}}{Flux_{ave}} \quad (9)$$

The shape of the chosen absorber is square, so height and width have the same value. Then it was chosen the limit angle, which causes the radiation reflected by the heliostats, placed beyond this limit, which does not reach the receiver; so a square limit has been selected. The azimuth orientation equal to 0° and a start value of 0° for the zenith orientation of the receiver (then optimized in the calculation software progress) have been set.

The horizontal and vertical acceptance angles, through which the receiver can accept the incident radiation, have been imposed equal to 180°. The thermal losses of the receiver of 71.72 kW/m2 have been calculated while the pressure losses of the tower are 0.77 %.

For the ray tracing, the Hermite method has been used and, to not damage the receiver and keep the highest possible efficiency of the system, the "image size priority" has been employed as a point focusing strategy.

This choice is important, in fact, due to the not regular flux distribution, there are very high thermal gradient that causes a decrease of the lifetime and efficiency of the receiver [22].

An offset value of 2.5 for edge- x and edge-y was selected while the horizontal and vertical flux grid resolution equal to 25 have been chosen.

To evaluate the incident flux, efficiency matrix, receiver dimension and solar field, several number of simulation have been performed; in particular, the start values of 2.3 m of length and height and a zenith orientation of 0° have been set. Then the receiver area remained constant, varying the height, length and the zenith orientation from -65° to -45° generating for each simulation, a new solar field layout.

3. RESULTS

3.1 Heliostats field parametric analysis results

In this section, it will be shown the solar field result obtained by solar pilot, used in Simulink/Matlab for the dynamic transient simulation of the system.

At first it will be illustrated the results obtained for the Type 3 heliostats for the three solar multiple analyzed, in design point, or rather azimuth 180° and zenith 76°.

Table 3. Type 3 heliostats field results

SM	1	1.1	1.2	1.3
Heliostats	206	223	241	257
Reflective area [m^2]	3163.5	3424.5	3701	3354.7
Receiver height [m]	1.8	1.8	1.7	1.8
Receiver length [m]	3	3	3.18	3
Optical total efficiency [%]	77.4	77.2	76.9	76.7
Tower height [m]	55.5	56.5	57.5	60

As it is possible to observe from table 3, increasing the SM, there is also an increase of the heliostats number, while the optical efficiency decreases due to the distance. In fact, becoming numerous the heliostats, consequently, it rises up the distance between the last heliostats row and the tower; this effect is a consequence of the interception effect.

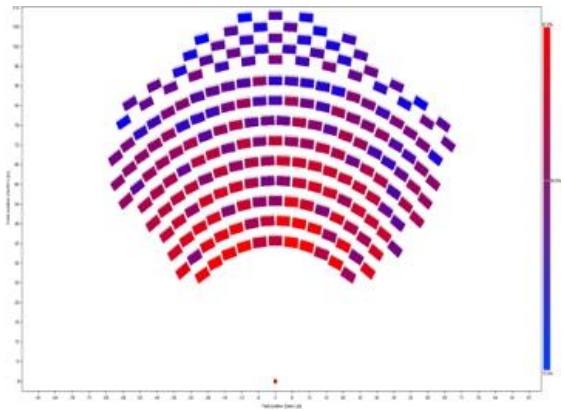

Figure 1. Solar field SM 1 Type 3 heliostats

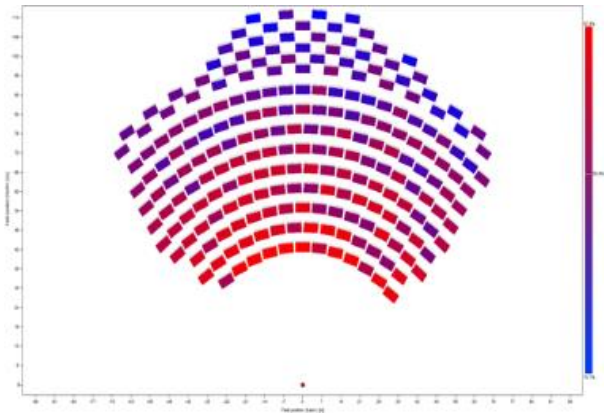

Figure 3. Solar field SM 1.2 Type 3 heliostats

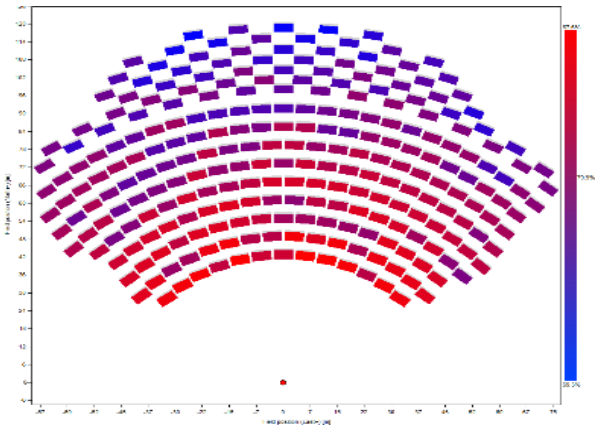

Figure 4. Solar field SM 1.3 Type 3 heliostats

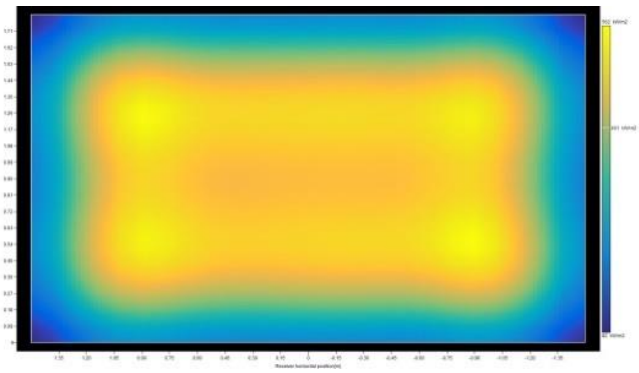

Figure 5. Incident flux on the receiver for SM 1 and heliostat type 3

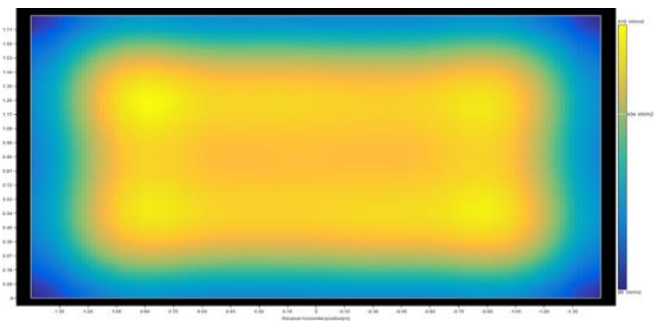

Figure 6. Incident flux on the receiver for SM 1.1 and heliostat type 3

In figure 1 it is shown the solar field for SM equal 1 with type 3 heliostats and in the others figures 2, 3 and 4 respectively for SM 1.1, SM 1.2 and SM 1.3.

As it can be seen, the maximum efficiency is related to the heliostats closest to the tower, i.e. for SM 1, and is 87.6%, while the minimum is relative to the heliostats farther from it and is 72%, for SM 1.3.

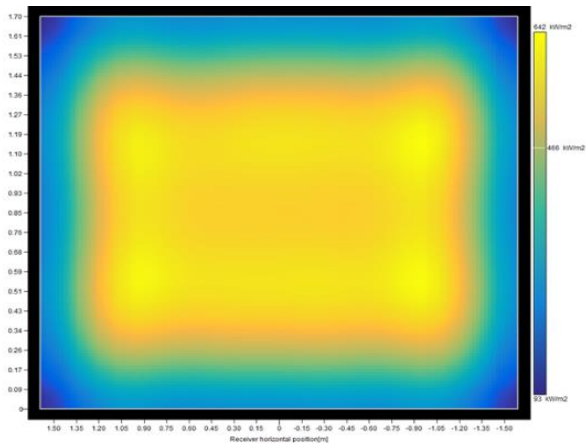

Figure 7. Incident flux on the receiver for SM 1.2 and heliostat type 3

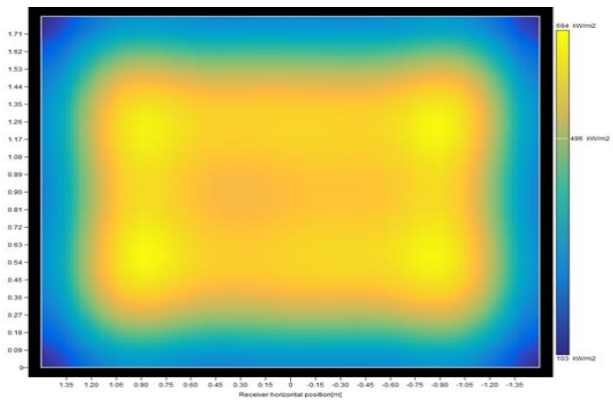

Figure 8. Incident flux on the receiver for SM 1.3 and heliostat type 3

Figures from 5 to 8 show the solar flux incident on the receiver surface for SM from 1 to 1.3 respectively, obtained with heliostats type 3. As can be observed, by increasing the solar multiple, there is an increase of both the average and the maximum flux, since the target point on the receiver shown in Figure 9 has been kept constant.

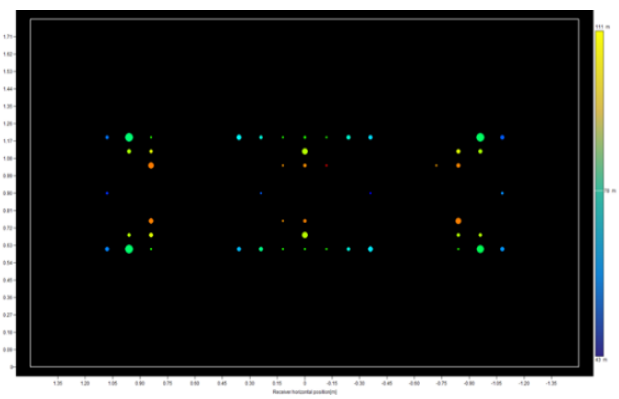

Figure 9. Aiming point of the heliostats chosen for the simulation

For all configurations, the maximum value of the solar flux is reached in areas aiming more heliostats; vice versa in areas with less aiming of heliostats, the solar flux is lower.

Table 4. Performance results of the solar fields for heliostats type 3

SM	1	1.1	1.2	1.3
Average heliostats field efficiency [%]	66.08	65.89	65.53	65.49

Table 4 resumes the annual average efficiency results obtained for heliostats type 3.

The following table 5 shows the results obtained for the type 2 heliostats, i.e. those of intermediate dimensions.

Table 5. Type 2 heliostats field results

SM	1	1.1	1.2	1.3
Heliostats	76	82	88	94
Reflective area [m^2]	3194.7	3446.9	3699.1	3951.3
Receiver height [m]	1.9	1.7	1.9	1.9
Receiver length [m]	2.84	3.18	2.84	2.84
Optical total efficiency [%]	77.4	77.1	76.8	76.6
Tower height [m]	54.5	56.5	57	58

As already noted for the type 3 heliostat, also for type 2 heliostat the increase in SM decreases the efficiency of the field due to the distance from the center of the tower. Table 4 shows these results.

The solar field layout for the heliostats type 2 are presented in figures from 10 to 13, for SM from 1 to 1.3.

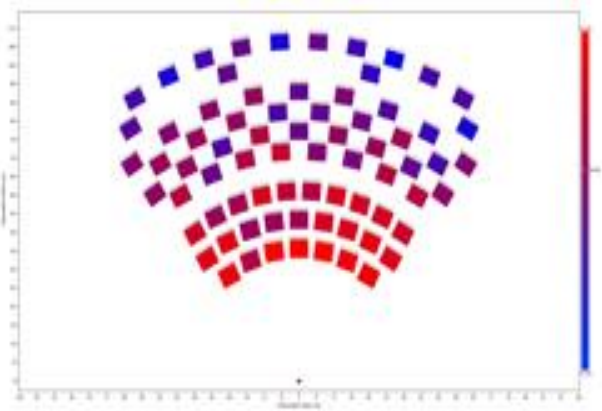

Figure 10. Solar field SM 1 Type 2 heliostats

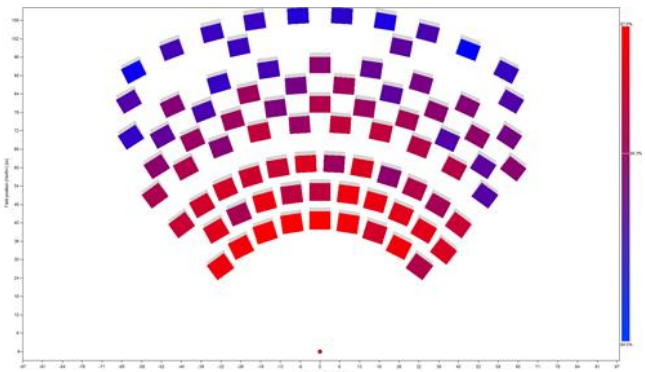

Figure 11. Solar field SM 1.1 Type 2 heliostats

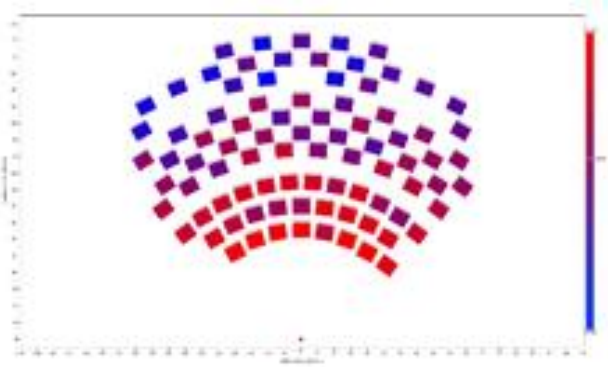

Figure 12. Solar field SM 1.2 Type 2 heliostats

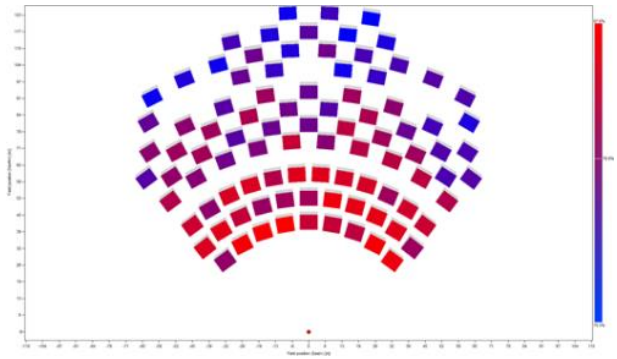

Figure 13. Solar field SM 1.3 Type 2 heliostats

The incident flux results for the heliostats type 2 are shown in figures from 14 to 17. As before mentioned, for heliostats type 2 the flux density dependents on the aiming point.

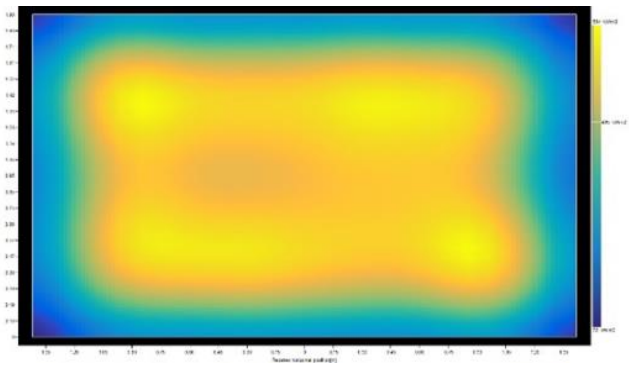

Figure 14. Incident flux on the receiver for SM 1and heliostat type 2

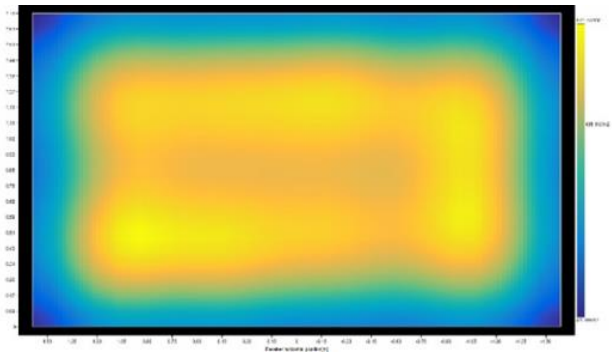

Figure 15. Incident flux on the receiver for SM 1.1 and heliostat type 2

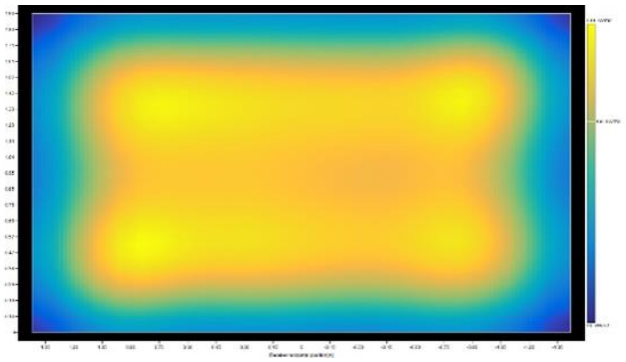

Figure 16. Incident flux on the receiver for SM 1.2 and heliostat type 2

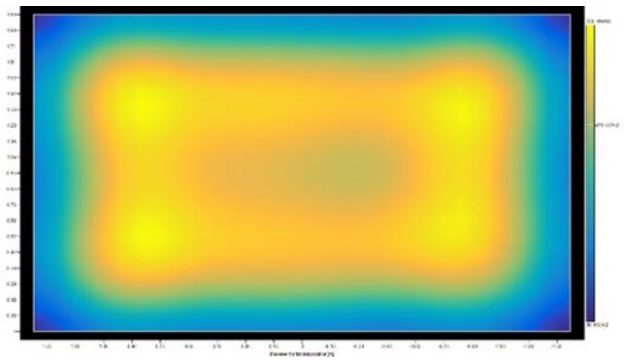

Figure 17. Incident flux on the receiver for SM 1.3 and heliostat type 2

Table 6. Performance results of the solar fields for heliostats type 2

SM	1	1.1	1.2	1.3
Average heliostats field efficiency [%]	64.83	64.15	64.21	63.96

Last heliostats type analysed is the type 1, i.e. the big one. The main results obtained for this kind of heliostats are summarized in table 7.

Table 7. Type 3 heliostats field results

SM	1	1.1	1.2	1.3
Heliostats	31	33	36	39
Reflective area [m2]	3443	3654.5	3986.7	4318.9
Receiver height [m]	2.6	2.5	2.4	2.4
Receiver length [m]	2.08	2.16	2.25	2.25
Optical total efficiency [%]	73.4	72.5	71.9	71.4
Tower height [m]	53.5	54.5	56	57

As it is possible to observe, the heliostats numbers, for each SM configuration, is low due to the high dimension of the heliostats, while the total optical efficiency decreases respect to the type 2 and type 3 cases.

It is interesting to observe how the reduction of the interception effect is substantial with the SM increase (2%), respect to the other two kinds of heliostats.

In the following figures 18, 19, 20 and 21 there are represented the heliostats field layout for all solar multiple analysed (1, 1.1, 1.2, 1.3).

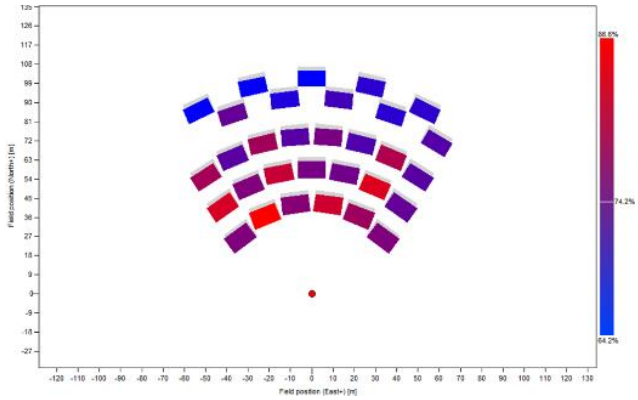

Figure 18. Solar field SM 1 Type 3 heliostats

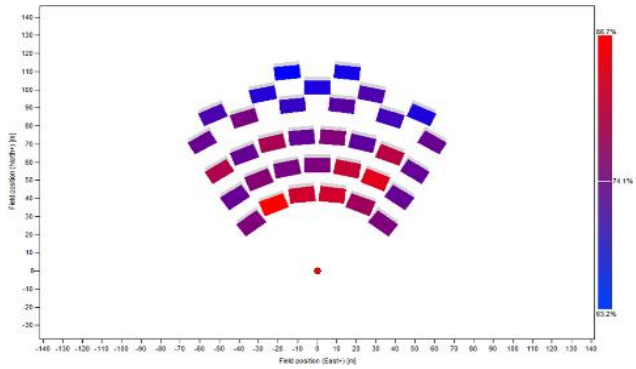

Figure 19. Solar field SM 1.1 Type 3 heliostats

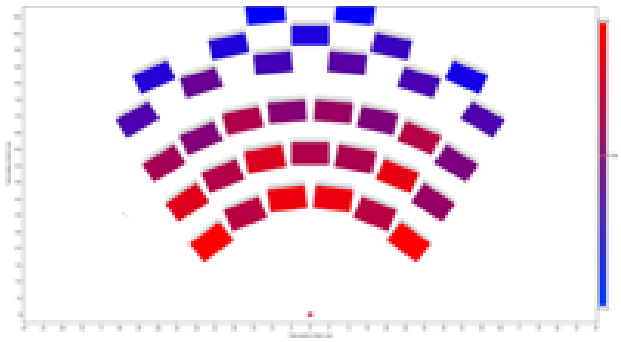

Figure 20. Solar field SM 1.2 Type 3 heliostats

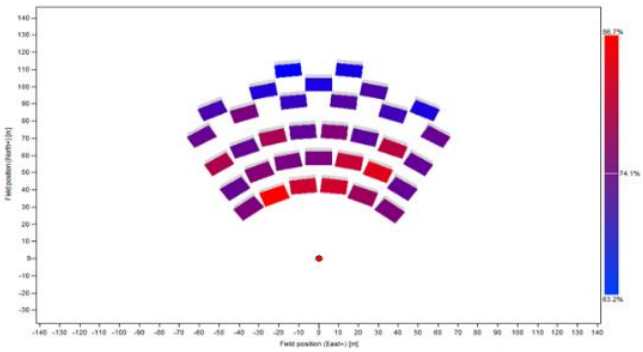

Figure 21. Solar field SM 1.3 Type 3 heliostats

In figure from 22 to 25 are represented the solar flux incident, for SM from 1 to 1.3.

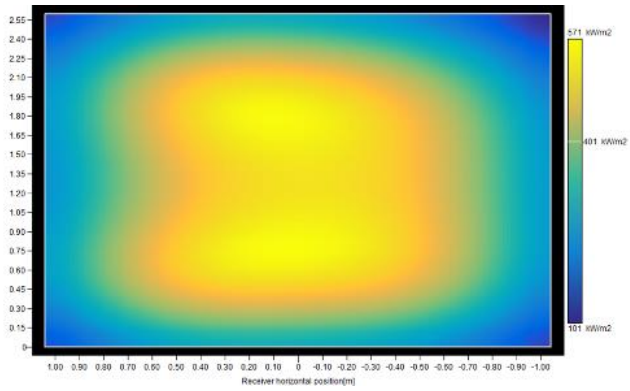

Figure 22. Incident flux on the receiver for SM 1 and heliostat type 3

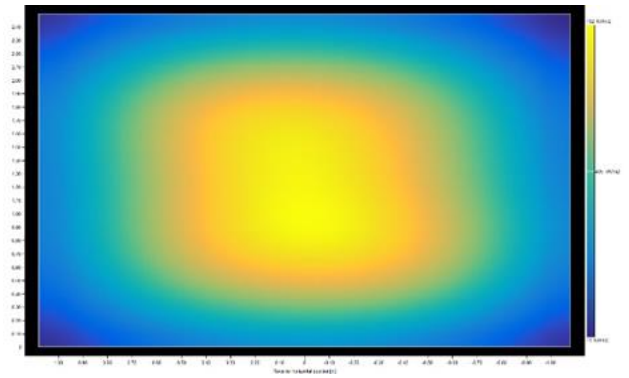

Figure 23. Incident flux on the receiver for SM 1.1 and heliostat type 3

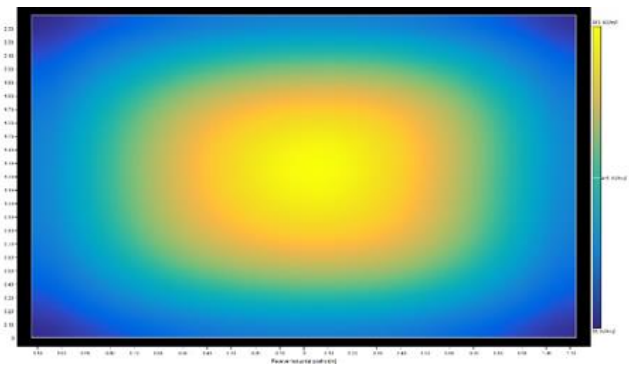

Figure 24. Incident flux on the receiver for SM 1.2 and heliostat type 3

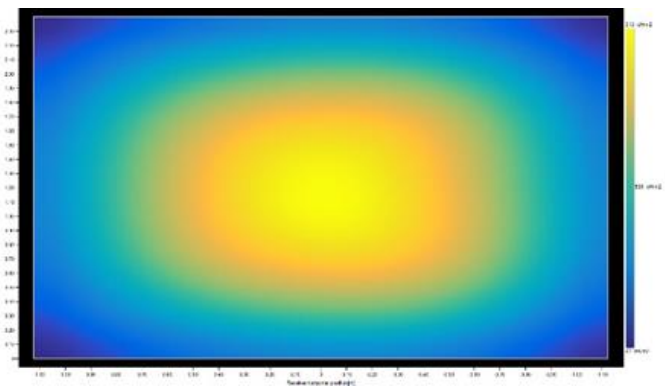

Figure 25. Incident flux on the receiver for SM 1.3 and heliostat type 3

Table 8. Performance results of the solar fields for heliostats type 3

SM	1	1.1	1.2	1.3
Average heliostats field efficiency [%]	59.38	58.85	58.1	57.49

3.2 Comparison of the results

In this part, the results obtained for the three kinds of heliostats will be compared. The comparison will be based on parameters as concentration ratio, total optical heliostats field efficiency, interception efficiency, annual average optical efficiency and receiver fluxes (average and maximum). Superscripts.

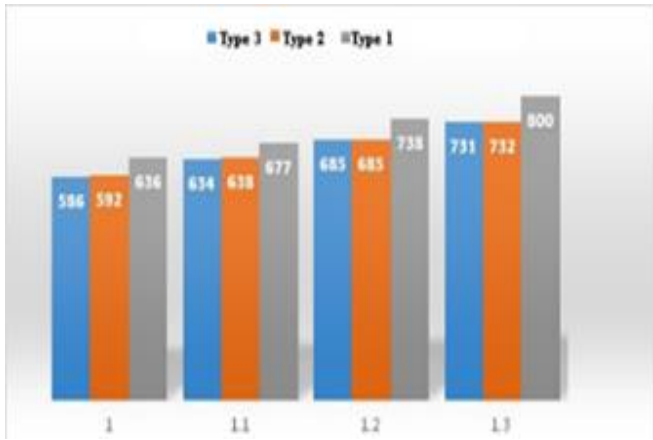

Figure 26. Concentration ratio for the three different kind of heliostats

From figure 26, it is apparent that the geometric concentration ratio increases as the solar multiple increases, for each heliostat size.

In addition, while the values for the small heliostats (type 3) and intermediate (type 2) are almost equivalent, the results for the heliostats of greater size (type 1), assume higher values.

Figure 27 shows the heliostats field optical. It can be noted that the efficiency decreases as the SM grows, due to the number of heliostats that are more distant from the tower, and thus have a lower efficiency.

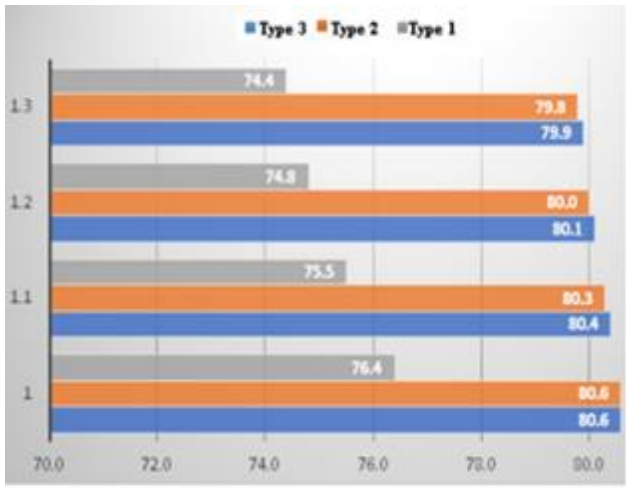

Figure 27. Heliostat field efficiency of the three size

Even in this case, type 1 has worse performance than the others. The value of lower optical efficiency is mainly determined by the interception effect, as shown in Figure 28.

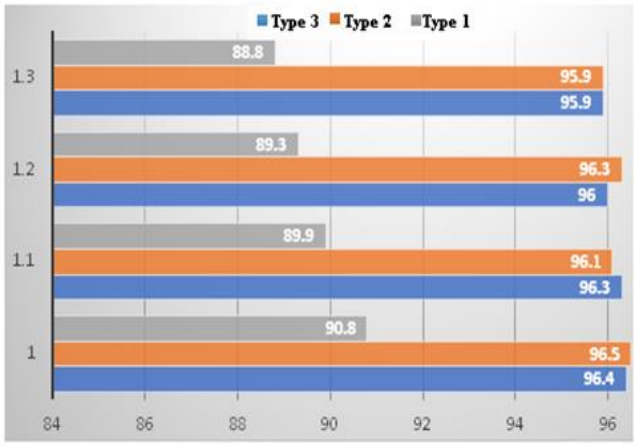

Figure 28. Interception effect of the heliostats type for the SM configuration analyzed

The interception effect is more evident for the heliostats type 1, because their size is greater than the one of the receiver (115.56 m2 against 5.4 m2)

The receiver is not big enough to intercept the entire image reflected by the heliostat, and part of the flux will be "spilled" by the edges.

Also for an annual efficiency, in the same way, there is the same effect as shown in Figure 29.

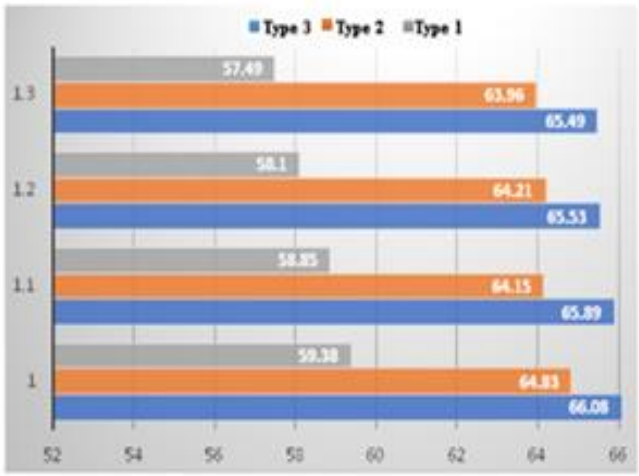

Figure 29. Annual efficiency for all configuration

3.3 Yearly simulation results

Table 9 resumes the energy production results, obtained in the yearly simulation of the numerical model, by Matlab/Simulink for the three kinds of heliostats for all solar multiple.

Table 9. Annual energy production [MWh]

SM	1	1.1	1.2	1.3
Type 1	0.90	0.94	0.99	1.03
Type 2	0.92	0.97	1.02	1.06
Type 3	0.94	1.00	1.04	1.08

As it is possible to observe, by increasing the SM, the energy increases, but the best energy production is for the heliostats type 3 (the smallest one), that allows the production of higher energy amounts.

The heliostats type 3 in heliostats field of SM 1.3 has the highest energy productions.

Figure 30 shows the energy production during the 21st of June for the three heliostats for SM 1.3.

The yellow line shows the performance of the biggest heliostat (type 1), the blue the ones of the intermediate and, finally, the green line the smallest one.

As it can be seen, the heliostats type 1 doesn't allow to control precisely the peak power; on the contrary, the type 3 makes the regulation of the power, together with the mass flow control system, more accurate around the nominal design point.

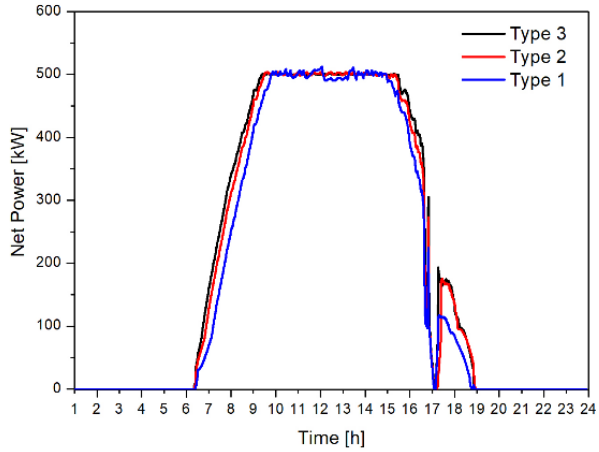

Figure 30. Heliostats types performances

Figure 31 depicts the performance of the heliostats type 3 for the three SM. It can be noted that the SM 1.3 allows to obtain the nominal power for a number of hours higher than the other configurations. Therefore, by this configuration, it is possible to increase the energy production.

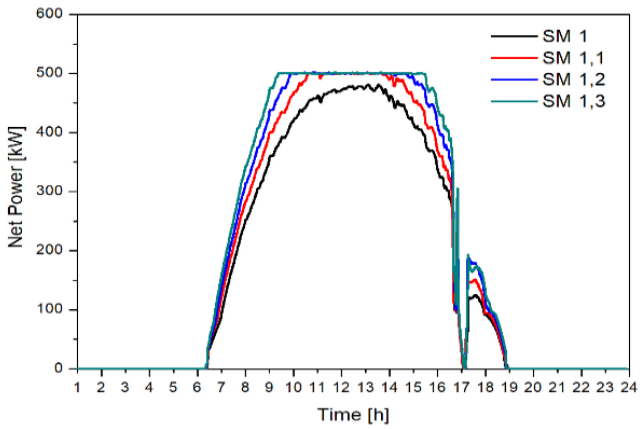

Figure 31. Heliostats type 3 performance for different SM

4. CONCLUSIONS

In this work, an optimization and design of the heliostat field has been carried out, for a micro solar turbine with a peak power of 500 kW, for three different sizes of heliostats and

four solar multiples. The power plant has two different logic of heliostat adjustments, in order to control the average incident flux of the receiver and the exceeding of TIT, and both are coordinated with the mass flow control system. The results show as the best configuration has SM 1.3, with small size heliostats; this allows to produce 1.08 MWh per year, and make a precise control of the peak power. Finally, this configuration represents the most suitable one for the mass flow control system employed in this kind of plant. The plant object of the present work does not use fuel; therefore, the optimization of the heliostats field has been performed with the aim of maximizing the conversion of solar energy. Energy production is sensitive to the efficiency of the field and therefore to the type of heliostats used.

ACKNOWLEDGMENT

Special thanks to Matteo Gallina for his precious support and to researchers of the Thermodynamics Department of University of Seville for their essentials suggests.

REFERENCES

[1] Noussan M, Roberto R, Nastasi B. (2018). Performance indicators of electricity generation at country level—the case of Italy. Energies 11(650). https://doi.org/10.3390/en11030650

[2] Ferraro V, Mele M, Marinelli V. (1975). Sky luminance measurements and comparisons with calculation models 73(13): 1780-1789.

[3] De Rosa A, Ferraro V, Kaliakatsos D, Marinelli V. (2008). Calculating diffuse illuminance on vertical surfaces in different sky conditions. Energy 33(11): 1703-1710. http://dx.doi.org/10.1016/j.energy.2008.05.009

[4] Lo Basso G, Nastasi B, Salata F, Golasi I. (2017). Energy retrofitting of residential buildings—How to couple combined heat and power (CHP) and heat pump (HP) for thermal management and off-design operation. Energy and Buildings 151: 293-305. http://dx.doi.org/10.1016/j.enbuild.2017.06.060

[5] Castellani B, Gambelli AM, Morini E, Nastasi B, Presciutti A, Filipponi M, Nicolini A, Rossi F. (2017). Experimental investigation on CO_2 methanation process for solar energy storage compared to CO_2-based methanol synthesis. Energies 10(855). https://doi.org/10.3390/en10070855

[6] Rovense F. (2015). A case of study of a concentrating solar power plant with unfired Joule-Brayton cycle. Energy Procedia 82: 978–985. http://dx.doi.org/10.1016/j.egypro.2015.11.855

[7] Rovense F, Amelio M, Scornaienchi NM, Ferraro V. Performance analysis of a solar-only gas micro turbine, with mass flow control. Energy Procedia 126: 675–682.

[8] Rovense F, Amelio M, Ferraro V, Scornaienchi NM. (2016). Analysis of a concentrating solar power tower operating with a closed joule Brayton cycle and thermal storage. International Journal of Heat and Technology 34(3): 485-490. http://doi.org/10.18280/ijht.340319

[9] Noussan M, Nastasi B. (2018): Data analysis of heating systems for buildings—a tool for energy planning, policies and systems simulation. Energies 11(233). https://doi.org/10.3390/en11010233

[10] Rovense F, Perez MS, Amelio M, Ferraro V, Scornaienchi NM. (2017). Feasibility analysis of a solar field for a closed unfired Joule-Brayton cycle 35(Sp.1): S166-S171. http://doi.org/10.18280/ijht.35Sp0123

[11] Amelio M, Beraldi P, Ferraro V, Scornaienchi M, Rovense F. (2016). Optimization of heliostat field in a thermal solar power plant with an unfired closed Joule-Brayton Cycle. Energy Procedia 101: 472-479. http://dx.doi.org/10.1016/j.egypro.2016.11.060

[12] Saito H, Latcovich J, Fusselbaugh M, Dinets M, Hattori K, Sakaki N. (2003). Microgas Turbine, Risks and Markets, IMIA Conference, Stockholm- September 2003.

[13] Technical Description T100 Natural Gas, T100 micro turbine system; D 14127-03 Version 3 09/12/29.

[14] AORA Tulip, Joining hands through sustainable energy for sustainable livelihoods; Overview of the Technology Solution. www.aorasolar.com. https://www.nrel.gov/SolarPILOT User Guide, 2016.

[15] Moreno TS. (2016). Solar resource assessment in Seville, Spain, statistical characterisation of solar radiation at different time resolutions. Solar Energy 132: 430-441.

[16] Segal A, Epstein M. (2001). The optics of the solar tower reflector. Solar Energy Supplement 6(69): 229-241. http://dx.doi.org/10.1016/S0038-092X(00)00137-7

[17] Téllez F, Burisch M, Villasente, Sánchez M, Sansom C, Kirby P, Turner P, Caliot C, Ferriere A, Bonanos CA, Papanicolas C. Montenon A, Monterreal R, Fernández J. (2014). State of the Art in Heliostats and Definition of Specifications, STAGE STE Projec, Deliverable 12.

[18] Ávila-Marín AL. (2011). Volumetric receivers in solar thermal power plants with central receiver system technology. Solar Energy 85(5): 891-910.

[19] Gomez-Garcia F, González-Aguilar J, Olalde G, Romero M. (2016). Thermal and hydrodynamic behaviour of ceramic volumetric absorbers for central receiver solar power plants: A review.

[20] Grobler A, Gauché P. (2014). A Review of Aiming Strategies for Central Receivers, in Proceedings of the second, Southern African Solar Energy Conference, Port Elizabeth, South Africa, 2014.

NOMENCLATURE

MGT	Micro Gas Turbine
DNI	Direct normal radiation [W/m^2]
SM	Solar multiple
CSPs	Concentrating Solar Power system
HTF	Heat Transfer Fluid
NREL	NationalRenewableEnergy Laboratory
TMY	Typical Meteorological Year

Greek symbols

ϕ	Solar radiation [W/m^2]
θ	Angular distance [°]